THE ASTROPHYSICAL JOURNAL, 404:584–592, 1993 February 20

IMAGING POLARIMETRY OF HIGH-REDSHIFT RADIO GALAXIES[1]

S. DI SEREGO ALIGHIERI
Osservatorio Astrofisico di Arcetri, Largo E. Fermi 5, 51025, Firenze, Italy
A. CIMATTI
Dipartimento di Astronomia, Università di Firenze, Largo E. Fermi 5, 50125, Firenze, Italy
AND
R. A. E. FOSBURY[2]
Space Telescope—European Coordinating Facility, Karl-Schwarzschild-Strasse 2, D-8046, Garching bei München, Germany
Received 1992 May 12; accepted 1992 August 27

ABSTRACT

We present the results of imaging polarimetry of six high-redshift radio galaxies. Four of them show high linear polarization in their rest frame ultraviolet radiation around 3000 Å with the E vector perpendicular to the radio/optical axis. In the only galaxy which is well resolved, the polarization is stronger in the extended structure than in the nuclear regions. These results are evidence for a significant nonstellar extended component in the ultraviolet band and are well explained by the hypothesis that this component is nuclear light which is emitted anisotropically and is scattered into our line of sight by the interstellar medium of the host galaxy.

Subject headings: galaxies: ISM — polarization — radio continuum: galaxies

1. INTRODUCTION

High-redshift radio galaxies (HZRGs) are characterized at optical wavelengths by elongated morphologies seen in both emission lines and continuum light and aligned with the radio axis (McCarthy et al. 1987; Chambers, Miley, & van Breugel 1987) suggesting that the optical and radio emission processes are closely related. This alignment is not present in the optical band at low redshift and has been explained as the effect of star formation induced by the ram pressure and shocks associated with the radio jet (Chambers, Miley, & van Breugel 1988). The mechanism for jet-induced star formation has been also investigated more quantitatively by some authors (De Young 1989; Rees 1989; Begelman & Cioffi 1989; Daly 1990). Two models have been developed within this scenario in order to estimate the ages of stellar populations. The first (Chambers & Charlot 1990; Bithell & Rees 1990) proposes that the entire stellar population is young and generated during a short-lived (about 10^8 yr), intense burst. Chambers & McCarthy (1990) have shown some evidence of OB star absorption lines detected in a spectrum obtained co-adding individual integrated spectra of a number of HZRGs, although at a low significance level. The second model (Lilly 1988, 1989) suggests that there are two distinct stellar populations: an old one which dominates in the optical-IR rest frame spectral region and produces the remarkable continuity and small scatter in the relation between the infrared K magnitude and the redshift, and a young one which is responsible for the UV rest frame light and for the alignment and whose importance is different from galaxy to galaxy.

New information on HZRGs came from polarimetric observations (di Serego Alighieri et al. 1989; Scarrott, Rolph, & Tadhunter 1990). Two HZRGs (3C 368 and 3C 277.2) show a highly polarized continuum in the ultraviolet rest frame spectral region, with degrees of linear polarization up to about 20% and electric vectors oriented perpendicular to the radio-optical axes. These observations provide evidence for a nonstellar component in the UV light from these objects. This component is explained as the result of the scattering of anisotropic radiation emerging from the nucleus of the galaxy and would be responsible for at least a fraction of the alignment effect. The scattering medium could be Galactic dust or free electrons from a hot halo or cooling flow (Syunyaev 1982; Fabian 1989; Wise & Sarazin 1990). This scattering model is related to the recent unifying schemes for active galactic nuclei (Orr & Browne 1982; Antonucci & Miller 1985; Barthel 1989; Padovani & Urry 1992 and references therein), since it implies anisotropic emission of radiation from the nucleus, and provides a tool for studying this emission even when it is not directed toward us.

Early observations performed with infrared arrays seemed to indicate that the alignment with the radio axis might be present also at longer wavelength (Eisenhardt & Chokshi 1990). However, recent infrared and optical observations of samples of HZRG (Rigler et al. 1992; McCarthy, Persson, & West 1992b) have shown that the alignment is strong only in the rest frame ultraviolet while the infrared morphologies, corresponding to rest frame wavelength around 1 μm, are much more symmetric. These results support strongly a two-component model for HZRG. The first component, predominant at longer wavelength ($\lambda_{\rm rest} \simeq 1$ μm), has the morphology, physical dimensions, and spectral energy distribution of giant elliptical galaxies which host powerful radio sources at low redshift. The second component, called *active* by Rigler et al. (1992), is aligned with the radio axis. It dominates in the UV rest frame region and has a roughly flat SED in f_ν between 2500 Å and 1 μm. The alignment effect is then a strong function of wavelength, and the combination of these two components explains the weaker alignment at longer wavelengths, the small elongation in the infrared being due to the much-diluted contribution of the active component.

The evidence for optical linear polarization in HZRGs has

[1] Based on observations obtained at the European Southern Observatory, La Silla, Chile.
[2] Affiliated to the Astrophysics Division of the Space Science Department, European Space Agency.

increased with the observations of the galaxy 3C 265 (Jannuzi & Elston 1990). Also the earlier spectropolarimetric observations of low-redshift radio galaxies made by Antonucci (1984) and the more recent infrared polarimetry of 3C 223.1 (Antonucci & Barvainis 1990) are relevant in this context, and scattering was indeed suggested to explain the polarization of 3C 234.

Impey, Lawrence, & Tapia (1991) have made unfiltered polarimetric measurements through a small fixed aperture of a sample of radio sources (radio galaxies, quasars, and BL Lac objects). All their measured radio galaxies, but one have $z < 0.3$, and several of the highest redshift ones have $P \sim 3\%$–5%. Recent observations of 12 radio galaxies covering a range in redshift from 0.2 to 0.85 by Tadhunter et al. (1992) show that the observed degree of polarization is a strong positive function of redshift when observed in a fixed waveband.

We present here the results of imaging polarimetric observations of a sample of HZRGs which are known to exhibit aligned structures. The aim is to investigate the universality of perpendicular polarization and to investigate further the relationships between the aligned, active component and the redder symmetric structure.

2. OBSERVATIONS AND DATA REDUCTION

The six HZRGs that we observed were drawn from previous surveys (Spinrad et al. 1985; Dunlop et al. 1989; McCarthy et al. 1990) giving preference to clearly resolved and elongated objects with good alignment between radio and optical morphologies and magnitudes brighter than about 22. The observations were carried out in 1991 June at the ESO 3.6 m telescope in La Silla using EFOSC (ESO Faint Objects Spectrograph and Camera) in its imaging polarimetry mode. The CCD used is a high-resolution back-illuminated RCA SID 503 with 1024 × 640 format and pixel size 15 μm corresponding to 0".337.

Imaging polarimetry is achieved by the use of a Wollaston prism inserted into the grism wheel which splits the incoming image into two subimages orthogonally polarized and separated by 20" (di Serego Alighieri 1989). In order to prevent problems of source overlap and to reduce the sky contribution, a 40" period slotted mask is used in the aperture wheel. The final image at the CCD focal plane consists of alternate orthogonally polarized strips. The galaxies in our sample have a sufficiently small angular size to be well contained in one strip. Standard broad-band filters were used in order to select the wavelength band. In the absence of a rotating half-wave plate, the parameters describing the polarization are determined by making observations at different instrumental position angles ϕ, rotating the whole EFOSC.

For the galaxy 1336+020, the redshift was unknown, and we also obtained a spectrum with a 1".5 wide slit in the spectral range 3600–7000 Å and with a dispersion of 23 nm mm^{-1}. The filters (BVR) were selected in order to observe the UV rest frame continuum in the range approximately 2000–4000 Å. The main characteristics of the objects and the parameters of the observations are listed in Table 1.

The seeing conditions were good, with values of FWHM ranging from 0".9 to 1".2. The photometric calibration was derived from spectroscopic and imaging observations of the spectrophotometric standard star LTT 7379 (Stone & Baldwin 1983). Finally, observations of the polarimetric standard star HD 164740 ($P = 7.0\%$ in the V band; Carrasco, Strom, & Strom 1973) provided a check on the level of instrumental polarization.

TABLE 1

OBSERVATIONS

Object (1)	Magnitude[a] (2)	Band (3)	z (4)	$\Delta\lambda_{rest}$ (Å) (5)	ϕ (6)	Exposure (s) (7)
3C 226.....	21.7(V)	B	0.818	2150–2700	190°	2400
					325	2400
					332	2400
1336+020	20.6	V	0.567	3150–3900	270	1800
					300	1800
					330	1800
3C 324.....	21.7	R	1.206	2500–3300	200a	1800
					200b	1800
					245	1800
					270	1800
					300	1800
					330	1800
	...[b]	V		2220–2800	200	1800
3C 435A.....	19.9	V	0.471	3330–4150	240	1800
					270	1800
					300	1800
2028−293	21.8	B	0.503	2600–3300	270	1800
					300	1800
					330	1800
	20.4	V		3300–4050	270	1800
					300	1800
2226−224	20.8	B	0.380	2830–3550	245	1800
					270	1800
					300	1800
					330	1800
	19.2	V		3520–4450	270	1200

[a] Magnitudes are obtained from our data and are in the band listed in col. (3), except for 3C 226.
[b] Nonphotometric conditions.

The data reduction was carried out with the ESO MIDAS system. After the usual bias- and dark-subtraction, nonuniformities were corrected using flat-fields obtained with the Wollaston prism, since the sensitivity of the CCD appears to depend on polarization. The sky was subtracted separately on the two orthogonally polarized strips by fitting a constant value to local sky level surrounding each object. The flux of each galaxy was measured by integrating on apertures selected in order to include the whole object or some clearly resolved components and carefully positioned on corresponding areas on the two strips by using the separation measured on starlike objects. In order to evaluate the parameters describing the linear polarization of the objects, i.e., the degree of linear polarization P and the position angle θ of the plane of vibration of the E vector, we define a quantity $S(\phi)$ for each instrumental position angle ϕ. $S(\phi)$ is equivalent to the component of the normalized Stokes parameters describing linear polarization along the direction ϕ. This quantity is defined as

$$S(\phi) = \left[\frac{I(\phi)/I(\phi + 90°)}{I_u(\phi)/I_u(\phi + 90°)} - 1\right] \Big/ \left[\frac{I(\phi)/I(\phi + 90°)}{I_u(\phi)/I_u(\phi + 90°)} + 1\right], \quad (1)$$

where $I(\phi)$ and $I(\phi + 90°)$ are the intensities of the object measured in the two beams produced by the Wollaston prism, and $I_u(\phi)$ and $I_u(\phi + 90°)$ are the average intensities of field stars, which are assumed to be unpolarized and are used to correct directly for the small instrumental polarization. These field stars are selected over a wide range of magnitudes in order to check for possible nonlinearities. Instrumental polarization values are always less than 1%, with typical values in the range of 0.3%–0.6%, and are not a function of magnitude. The parameter $S(\phi)$ is related to P and θ by

$$S(\phi) = P \cos 2(\theta - \phi) . \quad (2)$$

Therefore P and θ are evaluated by fitting a cosine curve to the observed values of $S(\phi)$. We emphasize that our method is free from the effects of any time variation of the observing conditions such as seeing and instrumental polarization because the value of $S(\phi)$ depends only on the ratio of intensities measured on the *same* frame. Uncertainties of P and θ were evaluated from the propagation to $S(\phi)$ and then to P and θ of the Poissonian noise relative to the object and to the sky background. We have also checked the correct alignment of the instrumental position angle ϕ using astrometric field stars and the direction of the split of the two perpendicularly polarized images. We find that the zero point of the position angle scale is accurate within 1°.

The formal degree of polarization obtained from the fit (2) requires a correction which takes into account the bias due to the fact that P is a definite positive quantity (Wardle & Kronberg 1974). When P is less than or equal to 2 times its uncertainty ($P/\sigma \leq 2$), we replace it with an upper limit equal to 3 σ (see Table 2).

3. RESULTS

We have obtained polarimetric measurements for six high-redshift radio galaxies with redshifts between 0.38 and 1.21. The results are presented in Table 2, which also lists the maximum contribution to the polarization expected for the

TABLE 2

POLARIMETRIC RESULTS

Object	R.P.A.[a]	O.P.A.[b]	P[c]	P_c[d]	σ_P[d]	θ[e]	$\Delta\theta$[f]	A[g] (arcsec^2)	P_{ISM}[h]
3C 226	144° ± 3°[i]	135° ± 3°[j]	12.5%	12.3%	2.3%	49° ± 6°	86° ± 7°	60	0.27%
1336+020 whole[k]	175 ± 2[l]	176 ± 3[m]	6.2	6.1	1.1	88 ± 5	88 ± 6	56	0.04
1336+020 N			9.1	8.7	2.6	78 ± 7	98 ± 8	8	
1336+020 C			3.6	3.4	1.1	87 ± 6	89 ± 7	11	
1336+020 ext[n]			11.5	11.0	3.1	89 ± 7	87 ± 8	45	
3C 324	71 ± 4[i]	94 ± 4[m]	18.2	18.0	1.6	16 ± 5	78 ± 6	30	0.27
3C 435A C+N+W	32 ± 3°	19 ± 2[m]	2.2	<3.6	1.2	138 ± 15	(119 ± 15)	107	0.46
3C 435A N			3.8	<5.7	1.9	107 ± 22	(88 ± 22)	13	
2028−293 (*B*)	182 ± 3[p]	155 ± 5[m]	5.0	4.4	2.3	71 ± 15	84 ± 16	44	0.49
2028−293 (*V*)			1.5	<4.8	1.6	78 ± 30	(77 ± 30)	84	
2226−224 C+W	109 ± 3[p]	104 ± 5[m]	2.4	<6.6	2.2	43 ± 14	(61 ± 15)	63	0.15
2226−224 W			2.1	<6.6	2.2	46 ± 14	(58 ± 15)	15	
2226−224 C			2.3	<4.5	1.5	172 ± 23	(68 ± 24)	17	

[a] Radio position angle.
[b] Optical position angle.
[c] Formal degree of polarization resulting from the fit.
[d] Degree of polarization corrected for the bias (if $P/\sigma \leq 2$, 3 σ upper limits are listed).
[e] Position angle of the electric vector.
[f] Difference between O.P.A. and θ.
[g] Solid angle of the aperture.
[h] Maximum Galactic polarization expected.
[i] McCarthy et al. 1987.
[j] Rigler et al. 1992.
[k] The whole galaxy (C + extended regions).
[l] Dunlop et al. 1989.
[m] This work.
[n] Extended regions (C excluded; see text).
[o] McCarthy et al. 1989.
[p] McCarthy et al. 1990.

interstellar medium of our Galaxy, estimated from the Galactic extinction (Burstein & Hiles 1982) and from the formula $P_{ISM}(\%) \leq 9.0E_{B-V}$. We assume always $H_0 = 50$ km s^{-1} Mpc^{-1} and $q_0 = 0$. Hereafter we define the spectral index α according to $S(\nu) \propto \nu^{\alpha}$.

3C 226.—Deep images of 3C 226 obtained by Rigler et al. (1992) show a morphology of the continuum in B band well-aligned with the radio axis. The morphology in the [O II] (3727 Å) line is more extended than the continuum, but the alignment with the radio axis is weaker. The radio map at 2″–8″ resolution of Jenkins, Pooley, & Riley (1977) does not show any significant correspondence of the radio emission with the optical structure, which is very compact. We measure a high integrated polarization in the *B* band (around 2400 Å), which does not contain strong emission lines. The *E* vector is perpendicular to the optical axis within 1 σ.

1336+020.—This galaxy was selected from the optical and infrared survey of 178 radio sources in the Parkes Selected regions made by Dunlop et al. (1989). It is a fairly large galaxy with an optical major axis angular extension of about 9″ corresponding to about 80 kpc. The optical morphology shows three components: the core C elongated along the radio axis, a bright component N to the north and a fainter diffuse emission in the southern region (Fig. 1*a*). Because the redshift was unknown, we obtained a spectrum through C and N. It shows three emission lines which we identify as [Ne V]3426 Å, [O II] 3727+3729 Å, and [Ne III] 3869 Å at a redshift of 0.567. Table 3 shows the emission-line fluxes and equivalent widths. Most of the emission-line radiation comes from the component N, rather than from the core, and both have a flat continuum between 2400 and 4400 Å. We made *V*-band polarimetry of the whole galaxy including the southern extension, of the core C and of component N separately (see Table 2). The degree of polarization is clearly higher in N than in C and is even higher in the extended parts of the object obtained by subtracting the core from the entire galaxy. In all cases the E vector is perpendicular to the optical axis. Emission lines contribute only 15% and 3.6% of the radiation in the *V* filter for component N and the core, respectively. If emission lines are unpolarized, then the polarization of the continuum is raised to $P_c = 10.2\%$ for component N and $P_c = 3.5\%$ for the core. Note the very small contribution coming from interstellar polarization (see Table 2), the smallest in the sample.

Figure 1*a* shows that the northern radio lobe overlaps with N although the astrometric errors do not allow us to claim a perfect correspondence.

3C 324.—The optical spectrum of 3C 324, studied by Spinrad & Djorgovsky (1984), shows a low ionization emission spectrum with a strong line of [O II], resolved in both space and velocity. The observation of faint objects near the galaxy suggests that 3C 324 is the dominant member of a high-redshift cluster of galaxies. It is the most polarized object in our sample, with an *R* band (around 2900 Å in the rest frame)–integrated polarization of 18% derived from six separate measurements at five different position angles. We find that the *E* vector is more closely perpendicular to the optical than to the radio axis. Co-adding the *R* images, we find a faint clump located at about 2.7 (~30 kpc) from the center of the galaxy and aligned with the optical major axis. However, this extension is too faint to allow separate polarimetry. We also obtained imaging polarimetry in the *V* band, but with a low signal-to-noise ratio and only at one position angle. The value of $S(\phi)$ in the *V* band (at $\phi = 200°$) is lower than 0.14. If the position angle of the *E* vector were the same as that in the *R* band, the degree of the polarization in the *V* band would be less than or equal to the one in the *R* band. In order to investigate the radio-optical correlations, we have compared the most recent radio maps at 1.5 GHz and at 4.86 GHz obtained by Pedelty et al. (1989) (see Fig. 1*b*). It can be seen that the eastern radio lobe is separated from the optical structure, while the western lobe partially overlaps with the western optical clump. The radio polarization measurements show that the electric vector at 1.5 GHz is roughly parallel to the radio axis, while it is approximately perpendicular at 4.86 GHz for both lobes (Pedelty et al. 1989) and the degree of polarization is about 2%–3% for the western lobe (Davis, Stannard, & Conway 1983).

2028−293.—This galaxy was selected from the survey made by McCarthy et al. (1990) of southern steep-spectrum radio galaxies from the Molonglo Catalog. It is a double-lobe radio source with a small lobe separation and aligned optical morphology. Our deepest *V* image shows a diffuse morphology without particular structures. We observed it in *B* (three angles ϕ) and *V* bands (two angles ϕ). The galaxy has a fairly low degree of integrated polarization possibly lower in the *V* band, at least judging from the formal value of *P* obtained from the sinusoidal fit. Also in this case the perpendicularity of the *E* vector is better with the optical than with the radio axis. The spectrum obtained by McCarthy et al. (1990) showed two emission lines ([Ne III] 3869 Å and [O II] 3727+3729 Å) which are out of the *B* filter range but within the *V* band. It should be noted that, in this case, the optical emission extends beyond the radio structure out to about 6″ (~50 kpc) (see Fig. 1*c*). Nevertheless, there is no clear optical counterpart to the radio lobes.

3C 435A.—This radio galaxy was discovered at a small projected distance from the powerful radio source 3C 435B (McCarthy, van Breugel, & Spinrad 1989), but the two objects are at different redshifts. The structure of 3C 435A in our deepest images shows three distinct components: the central one (C) and two fainter objects, one (N) located at about 5″ (~40 kpc) to the north and the other (W) at 4″ (~30 kpc) to the west, with a radio-optical alignment only for N (see Fig. 1*d*). There is also another component almost aligned with the radio axis and located at about 8″ (~60 kpc) south of C. Unfortunately, it lies at the edges of the field of view, and for this reason it was not accurately measurable in all position angles and so excluded from the polarimetry. In the absence of spectroscopic data, the two fainter objects N and W could be part of the same galaxy, companion galaxies or totally unrelated objects. However, we suggest that N is physically related to the main component C, since it is located along the radio axis, and we use it to define the optical axis. We separately

TABLE 3

EMISSION LINES IN 1336+020

Region	Line	Flux (10^{-16} ergs cm^{-2} s^{-1})	Observed Equivalent Width (Å)
Comp N	[Ne V] 3426Å	3.3	72
	[O II] 3727Å	5.8	132
	[Ne III] 3869Å	2.6	40
Core	[Ne V] 3426Å	1.4	22
	[O II] 3727Å	1.4	21
	[Ne III] 3869Å	1.1	15

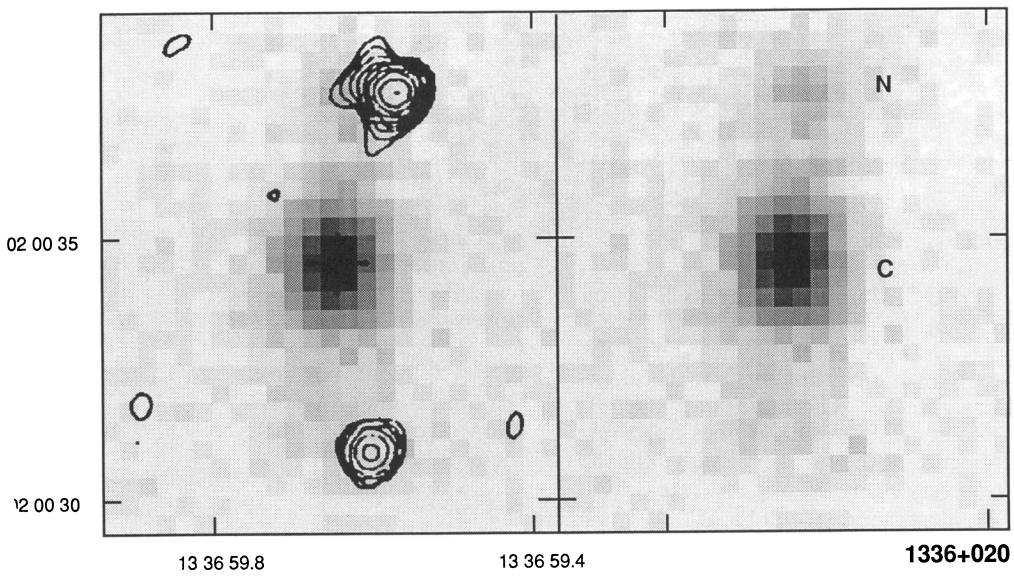

FIG.1*a*

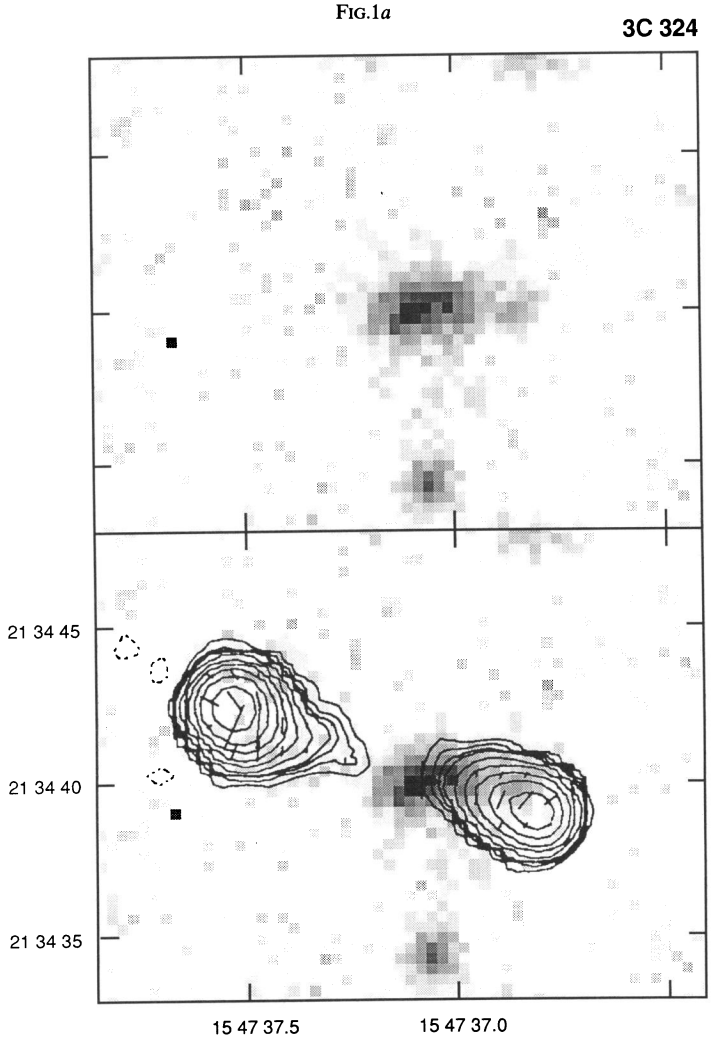

FIG. 1*b*

FIG. 1.—(*a*) The radio map at 5 GHz is taken from Dunlop et al. (1989), and we have overlaid our summed *V*-band image so that the galaxy core coincides with the optical astrometry by the same authors. This is the one case in our sample where there could be a spatial coincidence (within the astrometric uncertainies) between extranuclear radio and optical emission (component N). (*b*) The radio map (4885 MHz) is from Pedelty et al. (1989). Our *R*-band summed image is overlaid so that the peak of the optical core coincides with the optical astrometry of Gunn et al. (1981) used by Pedlety et al. Although the western radio and optical extensions are on a similar scale, it is unlikely that they actually coincide. (*c*) The radio map (4885 MHz) is taken from McCarthy et al. (1990). Our summed *V*-band image shows a diffuse emission extended to the southeast, and it does not show any evident clump. We overlaid the two images so that the optical brightness peak coincides with the astrometric position given by McCarthy et al. (1990). (*d*) The radio map at 1500 MHz is taken from McCarthy, van Breugel, & Spinrad (1989). Our *V*-band summed image has been overlaid so that the radio and the optical images of the angularly nearby quasar 3C 435 B (located at the lower left) are coincident. (*e*) The radio map (4885 MHz) is taken from McCarthy et al. (1990). Our *V*-band summed image has been overlaid so that the optical and the radio cores are coincident.

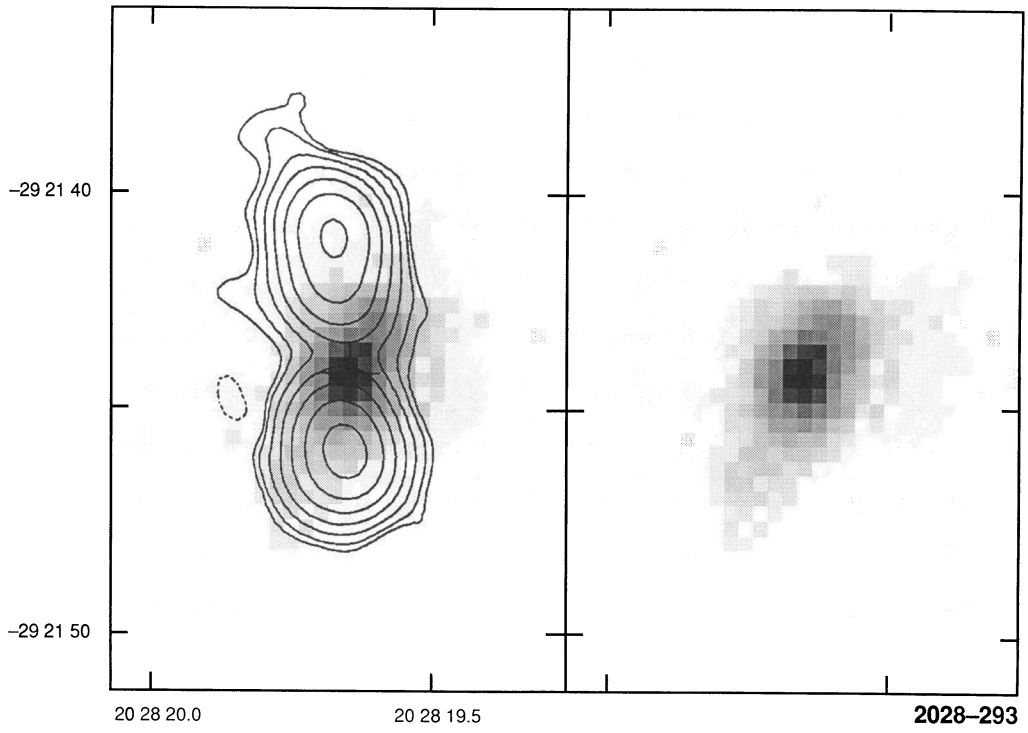

FIG. 1*c*

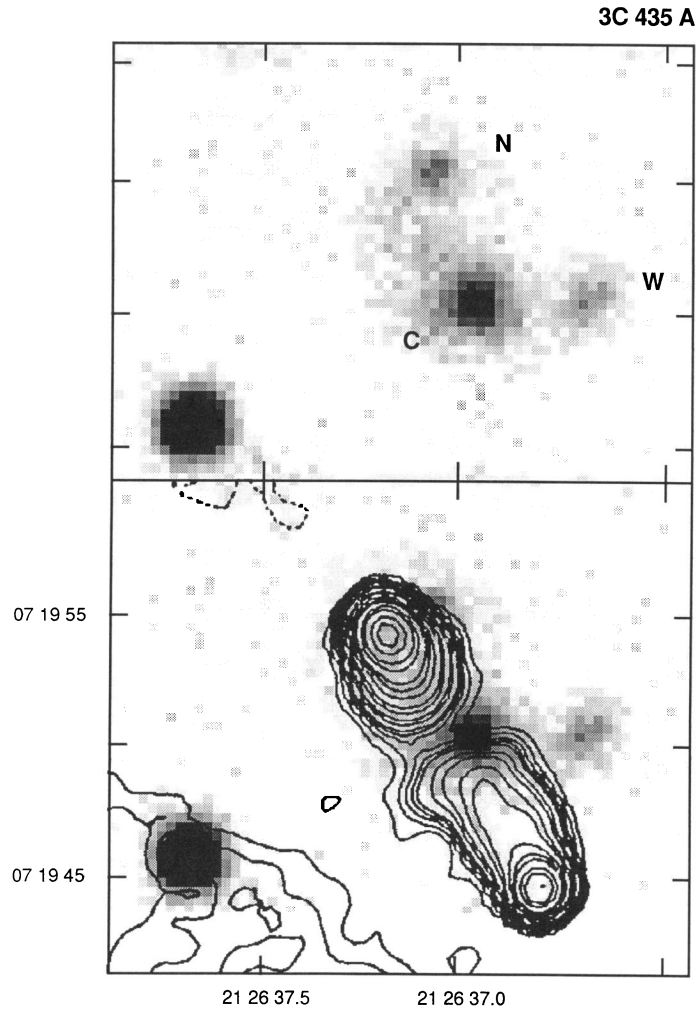

FIG. 1*d*

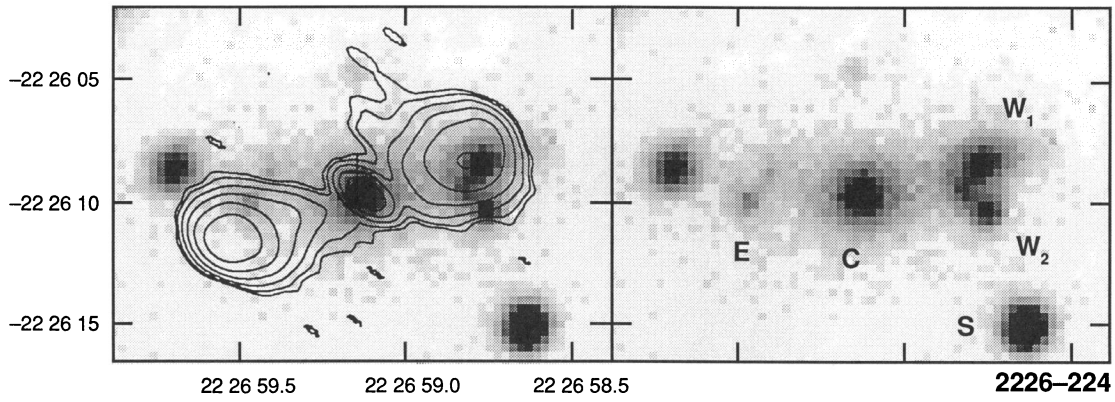

FIG. 1*e*

measured the degree of polarization of the whole object and of the single components in the V band. We obtain a good formal sinusoidal fit to $S(\phi)$ only for the whole galaxy (C + N + W) and the component N. The electric vector is approximately perpendicular to the direction from C to N. No reasonable fit can be obtained for C and W separately. Considering the large relative errors on P, we cannot regard 3C 435A as a clearly polarized galaxy and we give only upper limits to the degree of polarization. The radio map at 1.5 GHz (McCarthy et al. 1989) and the optical image overlay (Fig. 1*d*) is very accurate since it is based on the quasar 3C 435B and excludes a precise correspondence between the radio lobes and any of the optical components.

2226 − 224.—This galaxy was selected from the McCarthy et al. survey (1990). The optical counterpart having a total extension of 14″ (∼80 kpc) and $V = 19.2$ is made of three main components, E, C, and W (resolved into W1 and W2), roughly correlated with the triple radio source (see Fig. 1*e*). No emission lines were detected by McCarthy et al. (1990), and the redshift was estimated using the 4000 Å break and the Ca II H and K absorption lines. The component W2 has a profile similar to the one of the star S and could well be a foreground star, the counterparts of the radio source being limited to C, E, and W1, which are well aligned with the radio axis. The diffuse object at about 3″ to the east of component E has not been included in our measurements. We made polarimetry in the B band of C + W—since E is too faint to be visible in this band—and of C and W separately. The values of $S(\phi)$ obtained from the blue frames are consistent with a small polarization. Nevertheless, given the large relative errors, we can only give upper limits to the degree of polarization for this object. The only measurement in the V band gives values of $S(\phi)$ lower than the ones in B band. In the case of C + W, the ratio is $S_V(270°)/S_B(270°) = 0.23 \pm 0.02$.

4. DISCUSSION

We have performed imaging polarimetry of six radio galaxies with redshift between 0.38 and 1.21. High linear polarization (4%–18%) has been detected in the integrated light of four of the galaxies in a broad band corresponding to the rest frame ultraviolet around 3000 Å (see Tables 1 and 2). For the two remaining objects, we can only put an upper limit of about 5% on the linear polarization. In all cases, the plane of vibration of the E vector is perpendicular to the optical axis. Although all our objects have well-aligned radio and optical axes, the perpendicularity of the E vector is better with the optical than with the radio axis. In 1336 + 020, the only object for which we have spatially resolved polarimetry, the polarization is much stronger in the external parts than in the nucleus. In 2028 − 293 the polarization decreases at longer wavelengths, similar to 3C 368 (di Serego Alighieri et al. 1989).

The results presented in this paper significantly increase the number of radio galaxies at a redshift larger than 0.1 for which polarization measurements have been performed.

We make here a critical examination of the mechanisms which could produce the observed polarization. Instrumental polarization is excluded, since we have used field stars to normalize our measurements.

The possible contribution to polarization due to transmission through the interstellar medium of the Galaxy has been estimated using the values of Galactic extinction given by Burstein & Heiles (1982) and the relationship between the maximum interstellar polarization and the color excess (Serkowski, Mathewson, & Ford 1975): $P_{\rm ISM}(\%) \leq 9.0 E_{B-V}$. The results are listed in the last column of Table 2 and are fully consistent with the interstellar polarization measured by Mathewson & Ford (1970) for stars within about 2° of our objects. Furthermore, the perpendicularity of the E vector with the optical axis of the radio galaxy cannot be explained by the properties of Galactic dust. We conclude that the interstellar medium of our Galaxy makes a negligible contribution to the polarization.

Transmission through dust in the radio galaxy itself could in principle give high polarization. Perpendicularity of the E vector could be explained by a toroidal magnetic field around the radio axis. Nevertheless, the very high extinction expected from the amount of dust required is incompatible with the high Lyα/Hα ratio measured by McCarthy, Elston, & Eisenhardt (1992a) in two high-redshift radio galaxies, which implies $E_{B-V} \sim 0.1$. If the extinction in our objects is of the same order, transmission through dust cannot be the dominant contributor to polarization. In fact Spinrad & Djorgowski (1984) show that the emission-line ratios in 3C 324 are consistent with no reddening.

A further argument for considering it very unlikely that the interstellar extinction contributes a linear polarization of 10% or more is the fact that the observed spectral energy distribution (see, e.g., the flat f_λ of our continuum spectrum of 1336 + 020, equivalent to $f_\nu \propto \nu^{-2}$) allows only a small reddening; otherwise, the emitted spectrum becomes implausibly blue. For example, if the emitted spectrum is produced by stars, it cannot be bluer than the Rayleigh-Jeans part of a

blackbody spectrum, i.e., a power law with spectral index $\alpha_e = 2$; then for a standard extinction curve (Savage & Mathis 1979) the observed SED is a power law with $\alpha_o = \alpha_e - 3.45E_{B-V}$ (in the rest frame range $\lambda = 2500$–10800 Å). Since we observe $\alpha_o \sim -2$, using the empirical relationship for our Galaxy $P_{\rm ISM}(\%) \leq 9.0E_{B-V}$ (Serkowski et al. 1975), we obtain $P_{\rm ISM} \leq 10.4\%$. This is a conservative upper limit since the nonperfect coalignment of the grains over the whole galaxy and the likely presence of diluting unpolarized light would both decrease the integrated polarization. Therefore we exclude that the transmission through dust in the radio galaxy itself is the dominant contributor to the polarization, at least in the galaxies which are more strongly polarized.

High polarization has been observed in the optical counterparts of radio jets (Schlötelburg, Meisenheimer, & Röser 1988; Röser & Meisenheimer 1991) and hot spots (Röser 1989) and is due to synchrotron emission by high energy electrons travelling in a magnetic field. These optical structures are not only aligned with the radio axis but show an extremely good correspondence with the radio morphology both in surface brightness and polarization (see the review by Brindle & Perley 1984). This mechanism then cannot apply to most of our sources where such correspondence is not observed.

The only sources for which some of the optical emission overlaps with the radio structure are 1336+020, where the optical component N corresponds to the northern radio lobe (Fig. 1*a*), and 3C 324, where a faint optical emission corresponds approximately with the western radio lobe, which is also polarized at 4.86 GHz in the same direction as in the optical, although at a much lower level (Fig. 1*b*). Nevertheless, in both these objects, the observed optical brightness of the corresponding radio structures is well above what one can expect for synchrotron emission. In fact, in all known cases of radio-optical synchrotron radiation, the optical emission is below a simple extrapolation of the radio spectrum made with the radio spectral index (e.g., Röser 1989; Stiavelli et al. 1992; Sparks et al. 1992). We can then empirically set an upper limit to the optical synchrotron brightness corresponding to $V_{\rm sync} \geq 23.6$ for the component N in 1336+020 and to $R_{\rm sync} \geq 24.6$ for the western clump in 3C 324. Since the observed magnitudes are $V = 22.5$ ($V = 22.7$ for the continuum alone) and $R = 24.0$, respectively, synchrotron cannot be the dominant polarization mechanism in our objects. Furthermore, the integrated polarization of 3C 324 is so high that it cannot come only from the faint western clump, which contributes about 12% of the total light. The main body of the galaxy must be strongly polarized itself and its light cannot be due to synchrotron for lack of correspondence with the radio structure. We also remark that extended emission in radio galaxies is generally much bluer than expected for optical synchrotron emission which falls off rapidly toward the blue.

Recently Kartje & Königl (1991) have proposed that optical linear polarization of up to 10% can be induced in AGNs by scattering within the central funnel of thick accretion disk. Nevertheless this model foresees that the position angle of the polarization should be parallel to the radio jet and therefore cannot apply in our cases.

Finally, polarization could be due to a different scattering mechanism produced by more distant material when strong nuclear radiation is emitted preferentially along the radio axis, as foreseen by the schemes which propose to unify the various AGN types (e.g., Lawrence 1987; Barthel 1989; Padovani & Urry 1992 and references therein). Actually, if strong optical-UV radiation is indeed emitted anisotropically by active nuclei (see Antonucci 1989), any material, dust or electrons, along the "beam" would quite naturally shine as an elongated reflection nebula, dominating the optical structure of the objects not pointed toward us, especially at wavelength ranges where stars do not emit strongly. The observed polarization properties are all consistent with this scenario, which also explains the perpendicularity of the E vector with the optical axis. Since the scattering medium can be at large distances from the nucleus, the polarization is expected to be particularly strong in the extranuclear regions, where the dilution by direct nuclear and stellar light is smaller and the scattering geometry is better defined. This is indeed observed in the only HZRGs where these difficult observations have been possible: 3C 368 (di Serego Alighieri et al. 1989; Scarrott et al. 1990) and 1336+020 (presented here).

We stress that the lack of information on the extended polarization in the other objects is due to the faintness of the extranuclear regions and not to the fact that these are not polarized (see, e.g., 3C 265; Jannuzi & Elston 1991). In conclusion we believe that our scattering model best explains the observed polarization properties.

The nature of the scattering medium is still a matter of debate: di Serego Alighieri et al. (1989) have argued that the decrease of the degree of polarization with wavelength observed in 3C 368—and found here also for 2028−293—favors scattering by dust. Nevertheless in 3C 265 the polarization is constant with wavelength (Jannuzi & Elston 1991), and an intriguing infrared polarization has been observed in 3C 223.1 (Antonucci & Barvainis 1990). These cases could be explained with scattering by electrons. It is natural to think that the ISM around these galaxies contains both dust and electrons and that both contribute to scattering, although achieving sufficient Thomson optical depth may be difficult except in clouds very close to the nucleus.

The scattering of anisotropic nuclear radiation naturally accounts for the elongation and alignment observed in high-redshift radio galaxies especially in the rest frame ultraviolet. Increasing dilution by a normal stellar population explains the rounder morphologies observed around 1 μm (Rigler et al. 1992). The presence of young stars is not excluded by our observations, but they can be only one of the contributors to the rest frame UV light, and a careful evaluation of their importance relative to scattering is necessary before any conclusion can be drawn on the ages of these galaxies.

5. CONCLUSIONS

We have significantly extended the sample of high-redshift radio galaxies with polarization measurements. We observe high polarization in four of the six radio galaxies observed. In all cases the E vector is perpendicular to the aligned optical and radio axis and the degree of polarization is higher in the external parts for the only object where we have resolved polarization. Among the possible mechanisms, the one which can most consistently explain our results is scattering of anisotropic nuclear radiation by dust or electrons. Multiwavelength polarimetric observations will place constraints on the scattering medium and on the possible contribution from young stars to the rest frame ultraviolet. Deep absorption-line spectroscopy would be valuable for the determination of stellar populations in these galaxies.

A detailed model of dust scattering in an AGN and a critical review of all the polarization measurements of high-redshift radio galaxies will be presented in a forthcoming paper (Cimatti et al. 1993).

We wish to thank Marco Salvati for helpful comments and suggestions, Leslie Hunt and Rino Bandiera for reading the manuscript, and the anonymous referee for his useful suggestions.

REFERENCES

Antonucci, R. R. J. 1984, ApJ, 278, 499
———. 1989, in 14th Texas Symp. on Relativistic Astrophysics, ed. E. Fenyves (New York: NY Acad. of Science Press), 180
Antonucci, R. R. J., & Barvainis, R. 1990, ApJ, 363, L17
Antonucci, R. R. J., & Miller, J. S. 1985, ApJ, 297, 621
Barthel, P. D. 1989, ApJ, 336, 606
Begelman, M. C., & Cioffi, D. F. 1989, ApJ, 345, L21
Bithell, M., & Rees, M. J. 1990, MNRAS, 242, 570
Brindle, A. H., & Perley, R. A. 1984, ARA&A, 22, 319
Burstein, D., & Heiles, C. 1982, AJ, 87, 1167
Carrasco, L., Strom, S. E., & Strom, K. M. 1973, ApJ, 182, 95
Chambers, K. C., & Charlot, S. 1990, ApJ, 348, L1
Chambers, K. C., & McCarthy, P. J. 1990, ApJ, 354, L9
Chambers, K. C., Miley, G. K., & van Breugel, W. 1987, Nature, 329, 604
———. 1988, ApJ, 327, L47
Cimatti, A., di Serego Alighieri, S., Salvati, M., Fosbury, R. A. E., & Taylor, D. 1993, in preparation
Daly, R. A. 1990, ApJ, 355, 416
Davis, R. J., Stannard, D., & Conway, R. G. 1983, MNRAS, 205, 1267
De Young, D. 1989, ApJ, 342, L59
di Serego Alighieri, S. 1989, in 1st ESO/ST-ECF Data Analysis Workshop, (ESO Conf. and Workshop Proc. 31), ed. P. Grosbøl et al. (Garching bei Munchen: ESO), 157
di Serego Alighieri, S., Fosbury, R. A. E., Quinn, P. J., & Tadhunter, C. N. 1989, Nature, 341, 307
Dunlop, J. S., Peacock, J. A., Savage, A., Lilly, S. J., Heasley, J. N., & Simon, A. J. B. 1989, MNRAS, 238, 1171
Eisenhardt, P. R. M., & Chokski, A. 1990, ApJ, 351, L9
Fabian, A. C. 1989, MNRAS, 238, 41P
Gunn, J. E., Hoessel, J. G., Westphal, J. A., Perryman, M. A. C., & Longair, M. S. 1981, MNRAS, 194, 111
Impey, C. D., Lawrence, C. R., & Tapia, S. 1991, ApJ, 375, 46
Jannuzi, B. T., & Elston, R. 1991, ApJ, 366, L69
Jenkins, C. J., Pooley, G. G., & Riley, J. M. 1977, MmRAS, 84, 61
Kartje, J. F., & Königl, A. 1991, ApJ, 375, 69
Lawrence, A. 1987, PASP, 99, 30
Lilly, S. J. 1988, ApJ, 333, 161
———. 1989, ApJ, 340, 77
Mathewson, D. S., & Ford, V. L. 1970, MmRAS, 74, 139
McCarthy, P. J., Elston, R., & Eisenhardt, P. 1992a, ApJ, 387, L29
McCarthy, P. J., Kapahi, V. K., van Breugel, W., & Subrahmanya, C. R. 1990, AJ, 100, 1014
McCarthy, P. J., Persson, S. E., & West, S. C. 1992b, ApJ, 386, 52
McCarthy, P. J., van Breugel, W., & Spinrad, H. 1989, AJ, 97, 36
McCarthy, P. J., van Breugel, W., Spinrad, H., & Djorgowski, S. 1988, ApJ, 321, L29
Orr, M. J. L., & Browne, I. W. A. 1982, MNRAS, 200, 1067
Padovani, P., & Urry, C. M. 1992, ApJ, 387, 449
Pedelty, J. A., Rudnick, L., McCarthy, P. J., & Spinrad, H. 1989, AJ, 97, 647
Rees, M. J. 1989, MNRAS, 239, 1P
Rigler, M. A., Lilly, S. J., Stockton, A., Hammer, F., & Le Fèvre, O. 1992, ApJ, 385, 61
Röser, H.-J. 1989, in Hot Spots in Extragalactic Radio Sources, ed. K. Meisenheimer, & H.-J. Röser (Berlin: Springer-Verlag), 91
Röser, H.-J., & Meisenheimer, K. 1991, A&A, 252, 458
Savage, B. D., & Mathis, J. S. 1979, ARA&A, 17, 73
Scarrott, S. M., Rolph, C. D., & Tadhunter, C. N. 1990, MNRAS, 243, 5P
Schlötelburg, M., Meisenheimer, K., & Röser, H. J. 1988, A&A, 202, L23
Serkowski, K., Mathewson, D. S., & Ford, V. L. 1975, ApJ, 196, 261
Sparks, W. B., Fraix-Burnet, D., Macchetto, F., & Owen, F. N. 1992, Nature, 355, 804
Spinrad, H., & Djorgovski, S. 1984, ApJ, 280, L9
Spinrad, H., Djorgovski, S., Marr, J., & Aguilar, L. 1985, PASP, 97, 932
Stiavelli, M., Biretta, J., Møller, P., & Zeilinger, W. W. 1992, Nature, 355, 802
Stone, R. P. S., & Baldwin, J. A. 1983, MNRAS, 204, 347
Syunyaev, R. A. 1982, Soviet Astron. Lett., 8, 175
Tadhunter, C. N., Scarrott, S. M., Draper, P., & Rolph, C. 1992, MNRAS, submitted
Wardle, J. F. C., & Kronberg, P. P. 1974, ApJ, 194, 249
Wise, M. W., & Sarazin, C. L. 1990, ApJ, 363, 344